ORNL/TM-11390

ornl

OAK RIDGE NATIONAL LABORATORY

MARTIN MARIETTA

# Effects of Oblique Impact on Hypervelocity Shield Performance

E. D. Brewer
W. R. Hendrich
D. G. Thomas
J. E. Smith



OPERATED BY
MARTIN MARIETTA ENERGY SYSTEMS, INC.
FOR THE UNITED STATES
DEPARTMENT OF ENERGY

---

ORNL/TM--11390

DE90 006936

# DEFENSE AND SPACE PROGRAMS

Contribution from
Engineering Technology Division

# EFFECTS OF OBLIQUE IMPACT ON HYPERVELOCITY SHIELD PERFORMANCE

E. D. Brewer
W. R. Hendrich
D. G. Thomas
J. E. Smith



DATE PUBLISHED - JANUARY 1990

Prepared for
U.S. Air Force Weapons Laboratory
Kirtland Air Force Base
Albuquerque, New Mexico
under Interagency Agreement DOE No. 40-1663-A1

Prepared by the
OAK RIDGE NATIONAL LABORATORY
Oak Ridge, Tennessee 37831
operated by
MARTIN MARIETTA ENERGY SYSTEMS, INC.
for the
U.S. DEPARTMENT OF ENERGY
under contract DE-AC05-84OR21400

## TABLE OF CONTENTS

## LIST OF TABLES

# LIST OF FIGURES

## ABSTRACT

As part of the Advanced Shield Phenomenology Program, conducted from 1987 to 1989, a study of the effects of oblique impact on hypervelocity shield damage was performed. The specific threat used was an aluminum cylinder with a mass of 1.75 grams and a length to diameter ratio of one. Incidence angles of 30°, 60°, and 90° were studied. The same layered shield assembly was tested at the different incidence angles. Testing was performed at the Arnold Engineering Development Center, Arnold Air Force Base, Tullahoma, Tennessee. Hydrocode analysis of the interaction of the projectile with the front plate was performed for each of the different incidence angles.

Four conclusions from the study are summarized below:

1. Front plate damage from hypervelocity impact varies significantly with the incidence angle. Damage to the front plate was much greater at a 30° incidence angle than at a 60° incidence angle, and the minimum front plate damage for the three incidence angles compared occurred for the 90° impact case.

2. Damage internal to the shield results from two phenomena, the occurrence of spall debris from the back of the front shield directly behind the impact, and the penetration and breakup of the projectile along the original line of flight. The relative amounts, velocities, and spread of the debris from these two phenomena are also a function of incidence angle.

3. Back plate damage varies significantly with incidence angle. A layered composite shield which survives a normal impact may fail against the same projectile at a different incidence angle.

4. Debris generated external to the shield is also dependent on the incidence angle. Preliminary indications are that the damage potential of this type of debris increases as the projectile angle of incidence decreases.

Recommendations for further study on the effects of oblique impact on hypervelocity shield performance are given as part of this report.


## 1. INTRODUCTION

This report covers research done concerning the effects of projectile incidence angle on hypervelocity shield performance. This work was performed as part of the Advanced Shield Phenomenology (ASP) Program. Included here are the experimental work and supporting analyses, covering incidence angles of 30°, 60°, and 90°. Figure 1 shows the nomenclature used in specifying

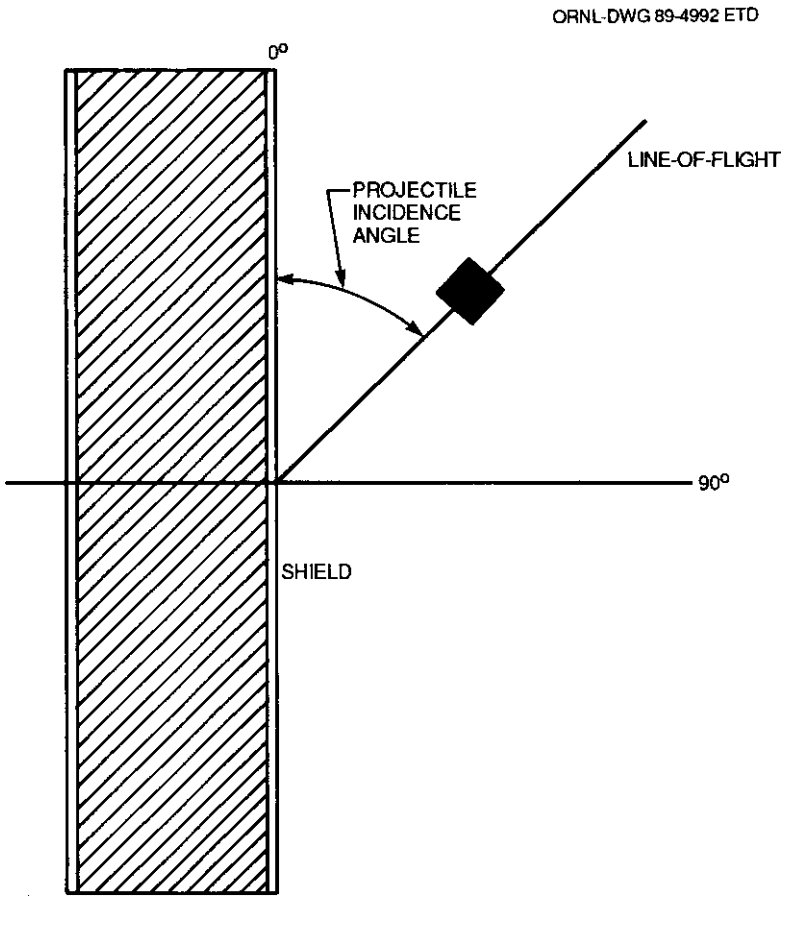


Figure 1. Angle nomenclature

the projectile incidence angle. The angle, as shown, is measured between the projectile line of flight and the surface of the front shield. The projectile used in shield testing was an aluminum cylinder with a mass of 1.75 grams and a length to diameter ratio of one. The impact velocity was 7 km/s. Testing consisted of firing a cylinder, as described above, into a layered shield assembly. For each test, the impact velocity was held constant at 7 km/s, but the orientation of the shield with the projectile line of flight was changed to provide the different incident angles. Shield hardware assemblies for the tests were identical, leaving the incidence angle as the sole variable. Experimental procedures, test hardware, and test results are covered in the correspondingly entitled report sections.

The hydrocode analysis covered in this report was performed after testing to provide further insight into the phenomenology under study. The Hull hydrocode was used to model 30°, 60°, and 90° impacts, using a cylindrical projectile in each case. Analytical methods and results are presented in the appropriate report sections.

Also included in this report is a brief survey of unclassified literature found on oblique impact effects, comparison of analytical and experimental results, conclusions reached as a result of this study, and recommendations for further work in this area.

## 2. LITERATURE REVIEW

Hypervelocity projectile impact into semi-infinite aluminum targets was studied by Cable (1965) for incidence angles from 20° to 90°. As the incidence angle decreased from 90° to 20°, crater depth, diameter, and volume all decreased. Incoming projectile kinetic energy can be divided into two components, with one component parallel and one component perpendicular to the target surface. Crater volume was shown to be proportional to the perpendicular, or normal, component of the projectile kinetic energy. Since the craters formed were essentially hemispherical, both the crater diameter and crater depth were proportional to the cube root of the normal component of the kinetic energy. These results are shown in Figure 2.

Summers (1965) studied oblique hypervelocity impact into thin structures. A very important part of his work was the observation of the complex spray pattern produced by oblique impact onto a thin shield. Material was observed to spall off perpendicular to the shield, and debris was also observed traveling along the original projectile path.

Later work by Gehring (1970) studied the effect of an oblique hypervelocity impact on the front shield on the damage to the back shield. Based on his assessment of back shield damage, he reached the following conclusions:

1. Peak impact pressure of the projectile on the front shield decreases as the incidence angle decreases from the 90° case.
2. Projectile fragmentation decreases along with the peak pressure and incidence angle.
3. The spread of the debris cloud behind the front plate (angle of dispersion) increases as the incidence angle decreases from the 90° case.

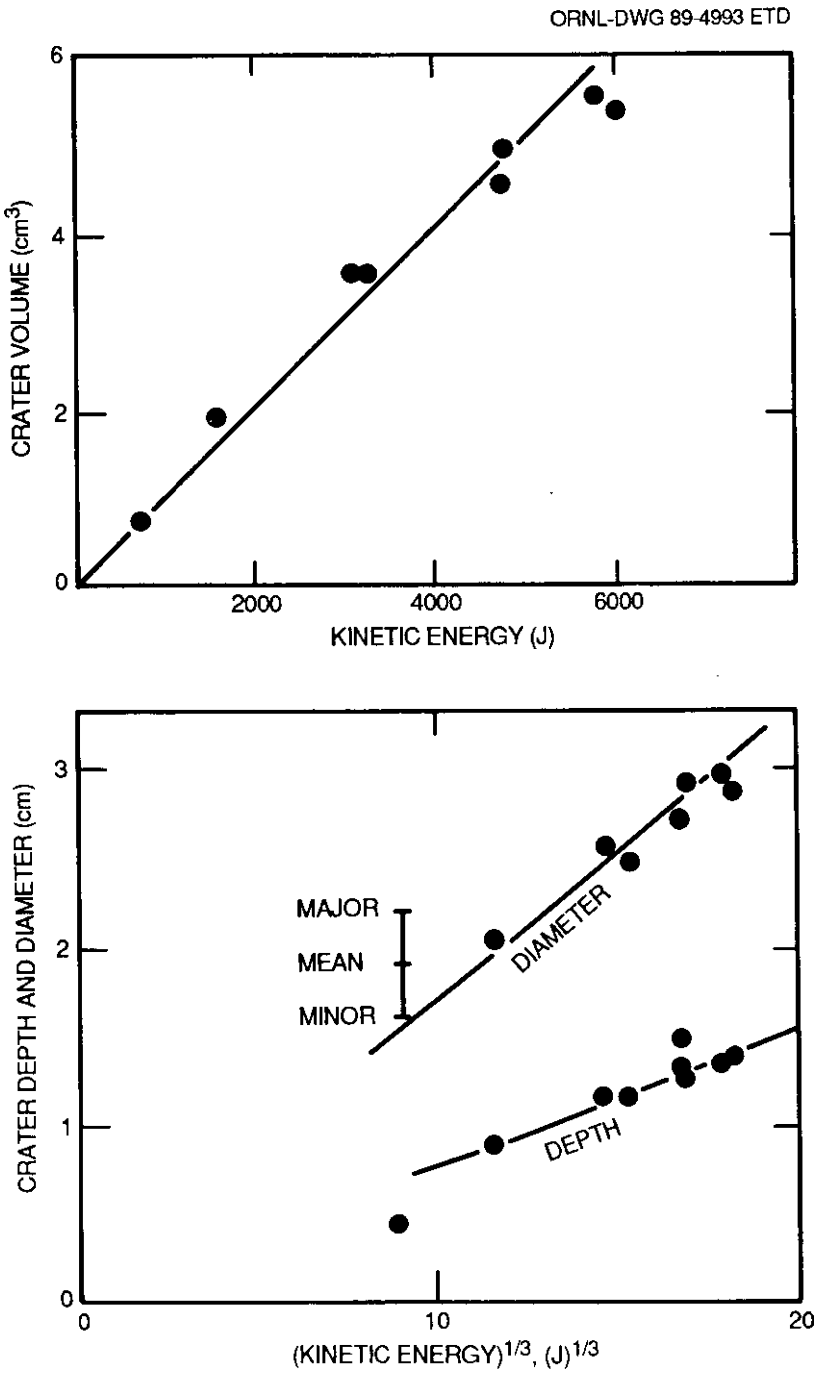


Figure 2. Crater parameters in semi-infinite aluminum (after Cable, 1966)

4. Back plate damage is at a maximum at an incidence angle of approximately 45°, as the spread of the debris offsets the effect of decreasing fragmentation.

Considering back plate failure, Gehring observed that:

1. Any shield which can survive low velocity fragmentation damage can survive oblique impact fragments.
2. Any shield which resists normal impact gross deformation tensile failure will not fail by that mechanism for oblique impact.

Debris clouds characteristics from oblique impact were studied by Orphal et al (1982) for the case of a stainless steel projectile onto a silica phenolic/aluminum composite. Target thickness to projectile diameter was kept constant at a ratio of 0.6, while the incidence angle was varied from 45° to 80°. These angles correspond to angles of 45° to 10° on Figure 1, as Orphal used a different convention and measured incidence angle from the shot line to a line normal to the target. For the conditions of the tests performed by Orphal et al. (1982), there was little reduction in the velocity of the debris cloud until the incidence angle was within 30° of the target surface. The velocity of the debris cloud was reduced to zero when the angle of the shot line was 10°, possibly indicating ricochet of the projectile. Reduction of the mass of material in the debris cloud began to be significant at an angle of 45° and also appeared to go to zero at an angle of 10°. These results are shown in Figure 3, again noting the different angle measurement convention.

Merzhievskii and Urushkin (1980) reviewed some of the phenomenology associated with oblique impact as well as conducting experiments with 2.3 mm diameter steel spheres impacting at 5 km/s. The spacing between the front and back shields of their study was 31 times the diameter of the projectile. Their results and discussions are summarized below.

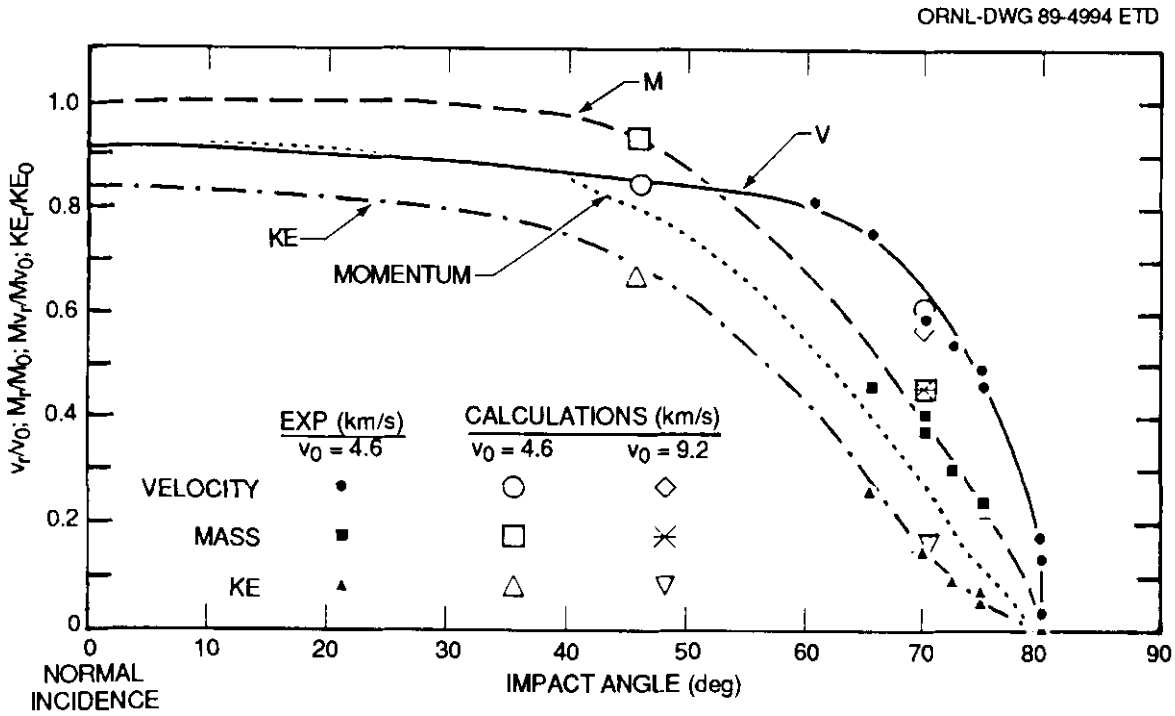


Figure 3. Residual debris cloud characteristics (after Orphal, 1982)

1. At oblique angles of impact, the impact phenomena which occur are more complicated than at normal incidence. High shear stresses occur in the projectile and the plate, with speeds much lower than the longitudinal shock waves generated. These stresses significantly affect the impact process, causing a different type of debris generation.
2. Front plate debris may be spalled off perpendicular to the plate due to a longitudinal shock wave generated at impact. Debris from the projectile continues on along the original projectile path. The resulting separation of debris from the plate and the projectile becomes more pronounced as the incident angle decreases.
3. The hole produced in the front shield was compared to an ellipse, with a minor axis equal to the hole created by an orthogonal impact of the same projectile at the same velocity. Using a simple geometric relation, the major axis of the elliptical hole produced was compared to

the minor axis divided by the sine of the incidence angle. The major axis was found to exceed this calculated value, by increasing amounts as the incidence angle decreased.

4. In evaluation of the velocity of the debris produced, there were three velocities considered: the shield debris velocity, the projectile debris velocity, and the maximum velocity orthogonal to the back plate (either the shield debris velocity or the product of the projectile debris velocity and the sine of the incidence angle). Relations were developed and compared to experimental data.
5. For oblique hypervelocity impact, projectile breakup phenomena are different from those occurring at normal impacts, and the results from normal impact studies cannot be extended to oblique impacts.
6. Further research is needed in the oblique impact area.

Schonberg et al. (1988) conducted oblique impact tests of aluminum spheres on aluminum plates at velocities from 5.0 to 7.5 km/s. The ratio of plate thickness to projectile diameter was from 0.20 to 0.33. This study included considerable analysis of the damage caused by debris generated which traveled external to the shield, called ricochet damage. One conclusion of this study was the existence of a critical angle, below which the damage was primarily external to the shield. Above this angle, closer to the orthogonal impact case, damage was primarily to the back shield. This angle was estimated to be between 30° and 25°, using the convention of Figure 1. Again, further research was recommended.

## 3. EXPERIMENTAL PROCEDURE

Testing was conducted at the Arnold Engineering Development Center at the Arnold Air Force Base in Tullahoma, Tennessee, using the S-1 Range Light Gas Gun. Several different types of data were recorded, working in coordination with the S-1 Range Personnel, including flash x-rays and strain gage readings. The detailed test and data acquisition methods are covered fully in a separate report devoted to that subject (Smith, in press) and are thus not included here.

The ASP Program included four test series (Series 4 through 7) over a period of three years, 1987 through 1989. The four shots covered in this report were part of Series 4, shots 39 and 41, and Series 5, shots 61 and 62. Series 4 was conducted in late 1987 and Series 5 in early 1988. For shots 39 and 41, the projectile line of flight was perpendicular to the shield surface, providing a 90° incidence angle. The standard test hardware setup, as used in the earlier test series of the ORNL Fast Track Program (ORNL Staff, 1989), was used for these tests. For shot 61, the angle of incidence was 30°. The test setup and holder hardware arrangement are shown in Figure 4.

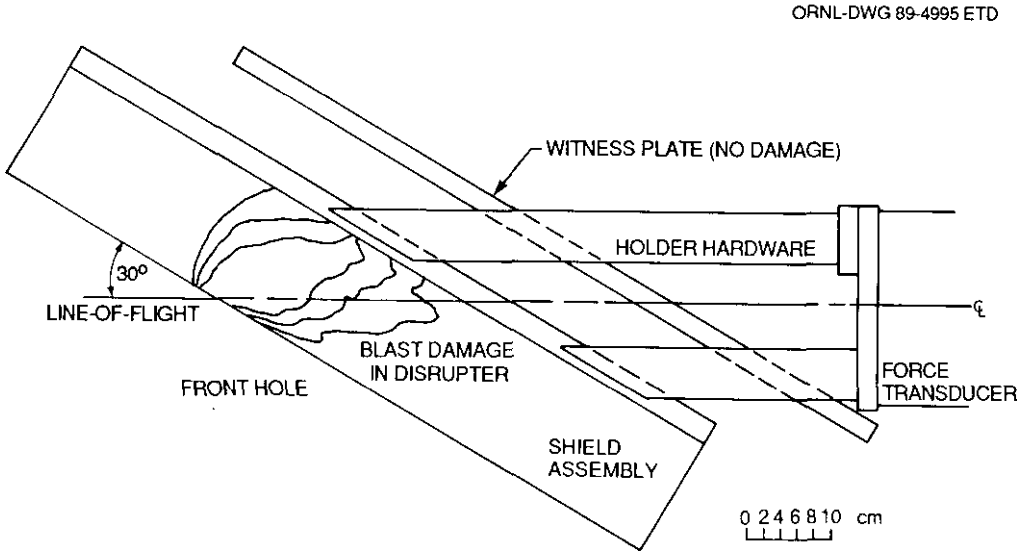


Figure 4. Test setup for shot 61

After shot 61, the holder hardware was changed. The setup for test 62, using an incidence angle of 60°, is shown in Figure 5. Impact velocity for both tests was 7 km/s. The projectile used was a 1.75 gram aluminum cylinder, with a length to diameter ratio of one.

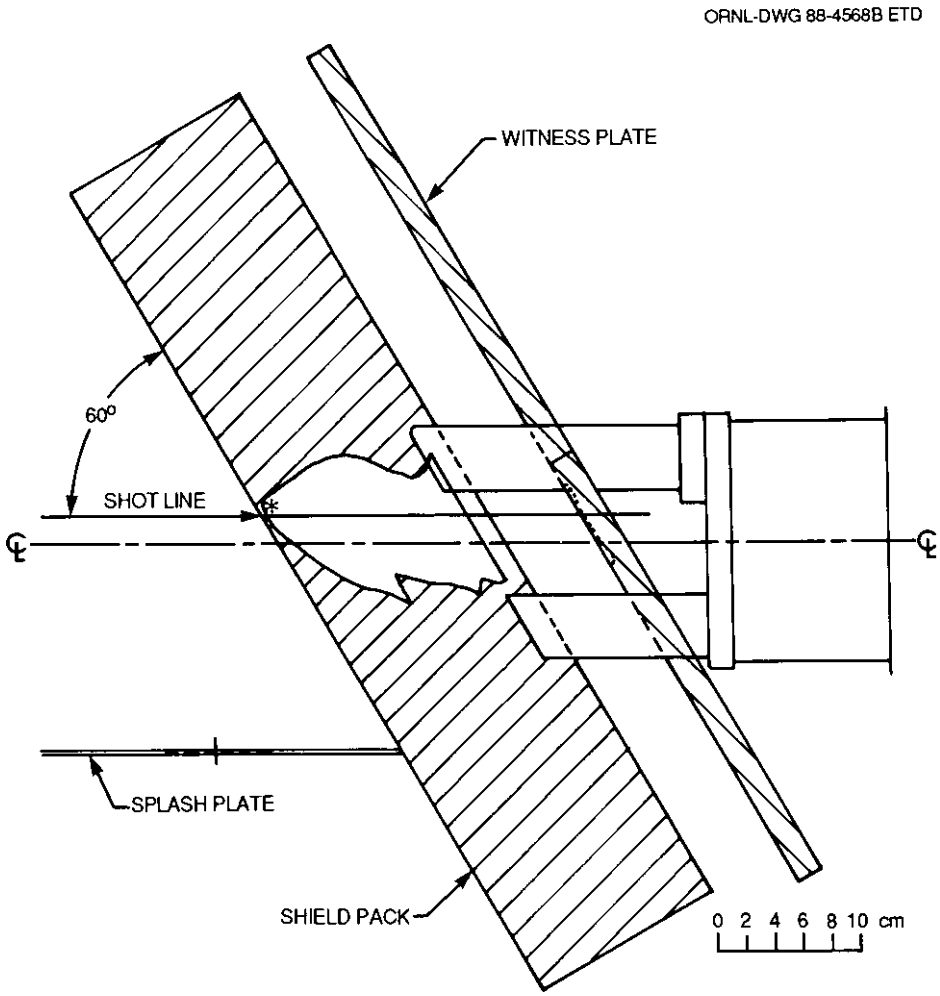


Figure 5. Test setup for shot 62

## 4. SHIELD TEST HARDWARE

Two normal impact shields are included in this study: (1) the homogeneous aluminum reference thickness to stop the aluminum projectile at 7 km/s with the back surface bulged but without spalling and (2) the lightest weight successful layered shield to stop the same threat. For the first of these two, shield 39, the solid shield was 7.87 cm of 6061T0 aluminum, areal density 21.4 g/cm$^2$. Shield 41 was composed of a 0.16 cm thick 2024T3 aluminum front shield, 0.97 gr/cm$^2$ carbon felt disrupter, and a back shield of 0.90 cm 304L stainless steel. With a 0.14 gr/cm$^2$ polyurethane spall catcher on the rear side of the back plate, the total areal density of shield 41 was 2.273 gr/cm$^2$. The shield hardware for shields 61 and 62 was identical to that of shield 41, with the exception of the omission of the spall catcher layer. [This layer was not necessary for the study of phenomena associated with oblique impact, primarily due to its location. For more information on the function and performance of the spall catcher layer, see the ORNL Fast Track Report (ORNL Staff, 1989).] Included behind the shields for shots 61 and 62, parallel to the back plate and 10.16 cm distant, was a 2.54 cm thick aluminum witness plate. These plates are visible in Figures 4 and 5. For shot 62, a "splash" plate was also included, to catch the debris generated external to the shield pack. This is shown in Figure 5.

## 5. TEST RESULTS AND DISCUSSION

The results for shots 39 and 41 are briefly covered here and are included in more depth in a separate report on a different portion of the ASP Program work (Thomas et al., in press). For reference, the solid aluminum shield had a definite bulge but no sign of spall. The layered configuration used for shot 41 (61 and 62 also) showed a definite overall back plate bulge, approximately 2 1/2 cm high, with no penetration. This success at 90° was the reason for the selection of this configuration to be tested at the oblique incidence angles.

The front plate damage for shields 61 and 62 is shown in Figure 6. Front plate holes generated by oblique impact are dependent on the incidence angle as well as such variables as front plate thickness and projectile diameter. To study the results due to incidence angle effects only, the front plate hole produced by an oblique impact can be normalized by the front plate hole produced under the same conditions but with a 90° incidence angle. This was done for the data given by Schonberg et al. (1987), Merzhievskii and Urushkin (1980), and the results of another ORNL

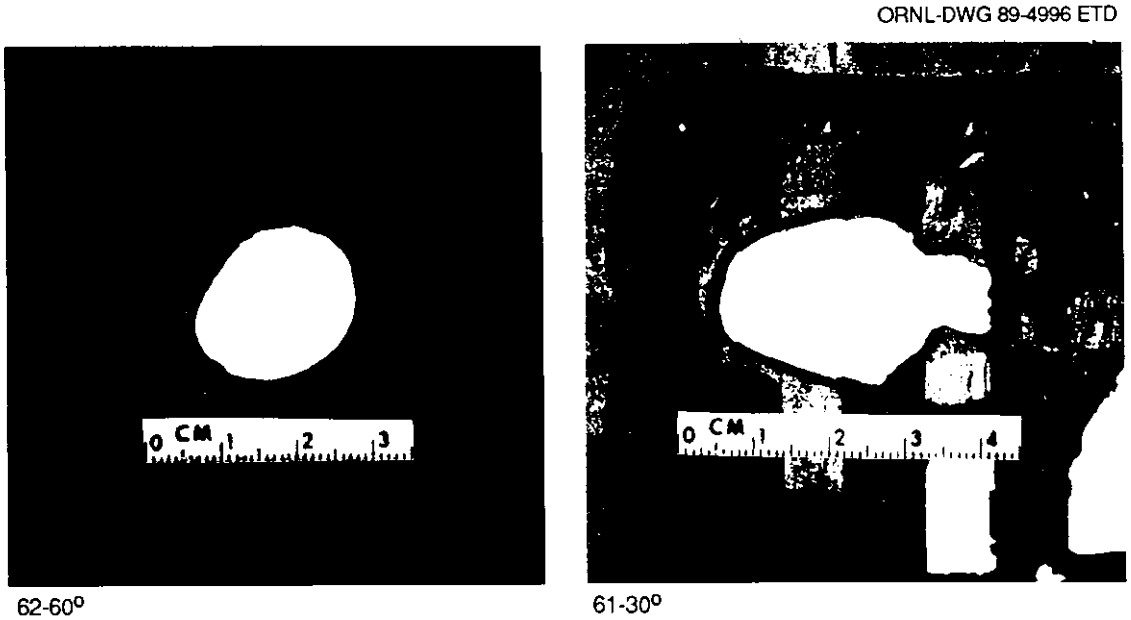


Figure 6. Front plate damage for shields 61 and 62

study (Thomas, 1988). These results are shown in Figure 7. The curve 1/sin a, where a is the incidence angle, is based on simple geometric considerations and the following assumptions:

1. A circular hole for a 90° impact and an elliptical hole for non-orthogonal incidence angles.
2. The diameter of the circular hole is equal to the minor axis of the ellipse.

Using A as the minor axis and B as the major axis of the ellipse, then

$$\frac{\text{area ellipse}}{\text{area circle}} = \frac{\text{pi/4 * A * B}}{\text{pi/4 * A * A}} = \frac{B}{A} .$$

By the geometry of the impact situation and assuming the elliptical hole is created by the same "cookie cutter" that created the 90° hole,

$$\frac{B}{A} = \frac{1}{\sin a} ,$$

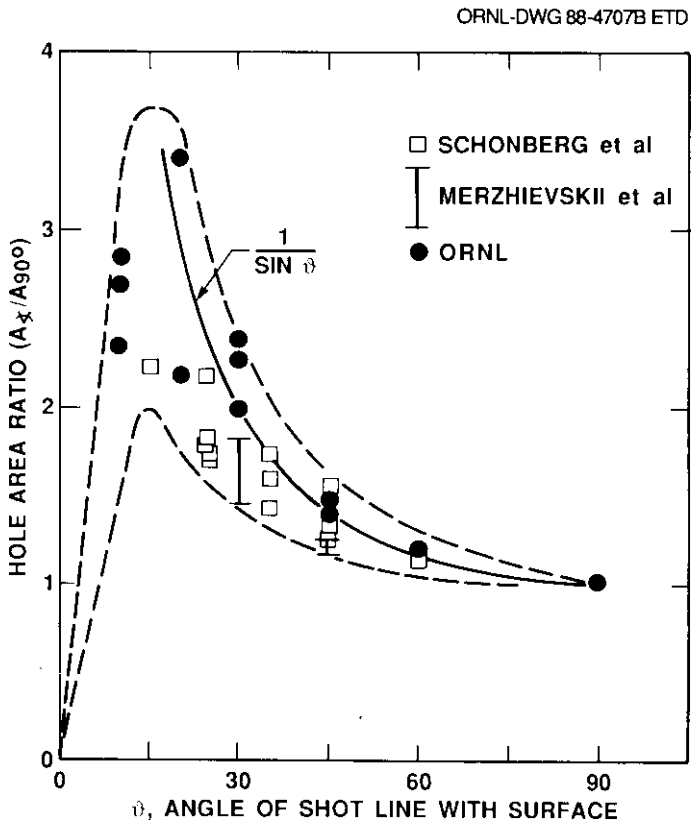


Figure 7. Front plate hole area versus incidence angle

as illustrated in Figure 8. For the case of a cylindrical projectile, the "cookie cutter" assumption includes the assumption that the projectile axis is oriented along the projectile line of flight. The results shown in Figure 7 show two interesting trends: (1) the approximation of 1/sin a is fairly accurate for angles above 15 to 20 and (2) the scatter of the results increases as the angle of incidence decreases.

To obtain information on the spread of debris behind the front plate, a careful examination and evaluation was made of the blast damage profile in the disrupter layers. The spread and intensity

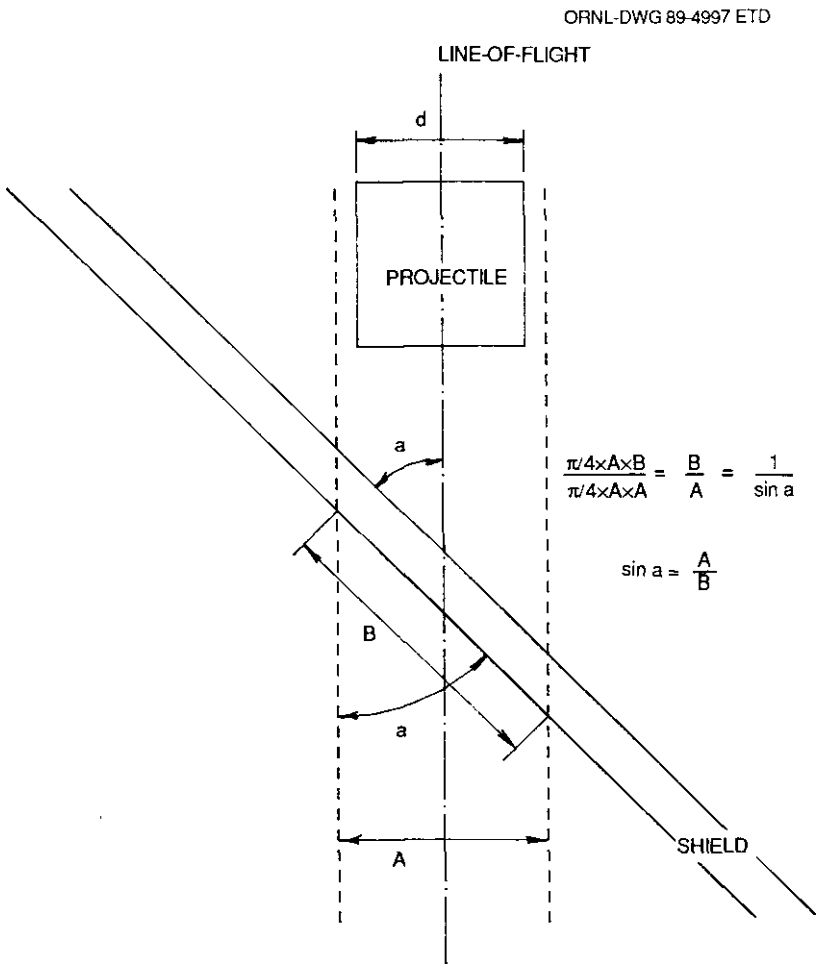


Figure 8. Geometry of "cookie cutter" approximation

of the damage in the disrupter layers gives information on the amount, direction, and source of the debris. Each shield disrupter pack was examined by layer in posttest disassembly, and the damage pattern noted. Three observations were recorded:

1. The minimum dimension of the main hole in the layer.
2. The maximum dimension of the main hole in the layer.
3. The maximum spread of any blast damage such as pinholes or tears in the layer.

These results are shown in Figure 9 for shot 61 and Figure 10 for shot 62. Also shown on these figures are the line of flight of the projectile and its continuation into the shield, the line of maximum damage, and a normal line into the shield from the point of impact. Examination of the damage for shield 61 (30° incident angle) shows a wide spread of blast damage, from spall and from penetration. The two effects are approximately equal, possibly with a slight preponderance of

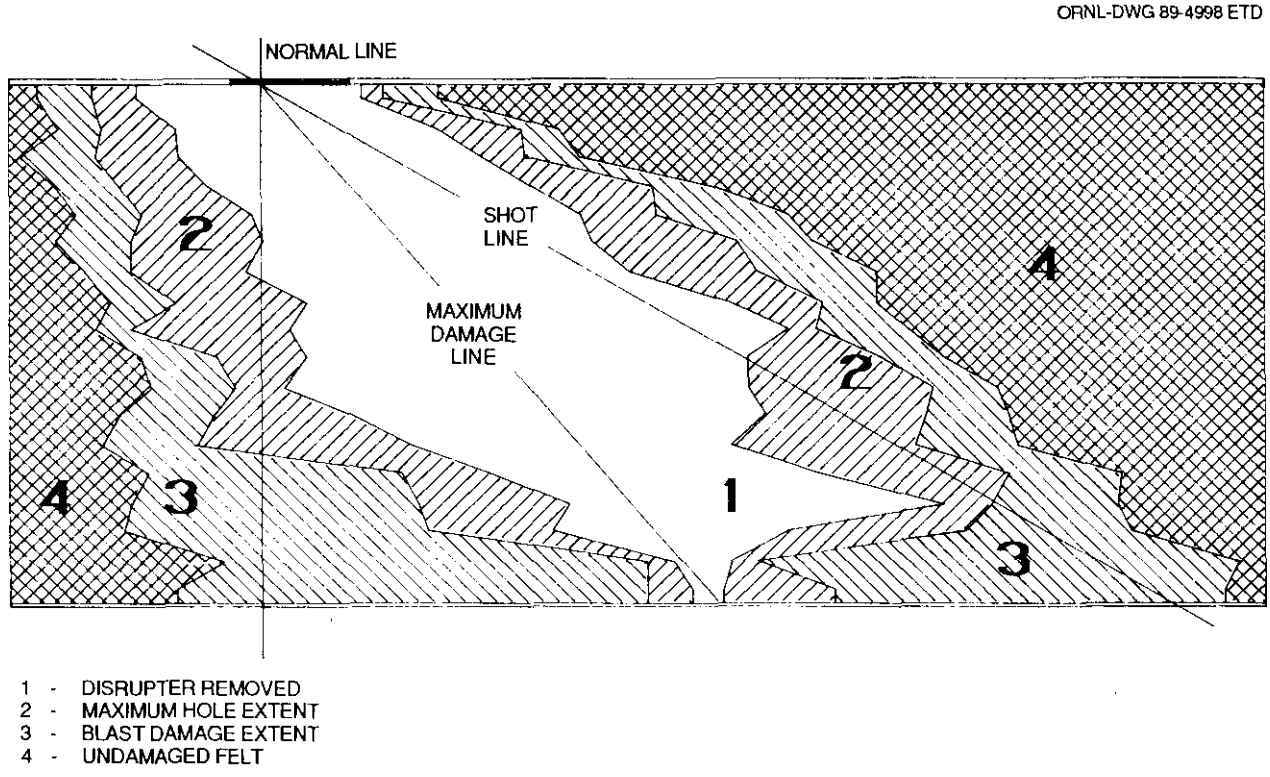


Figure 9. Disrupter blast damage profile for shot 61

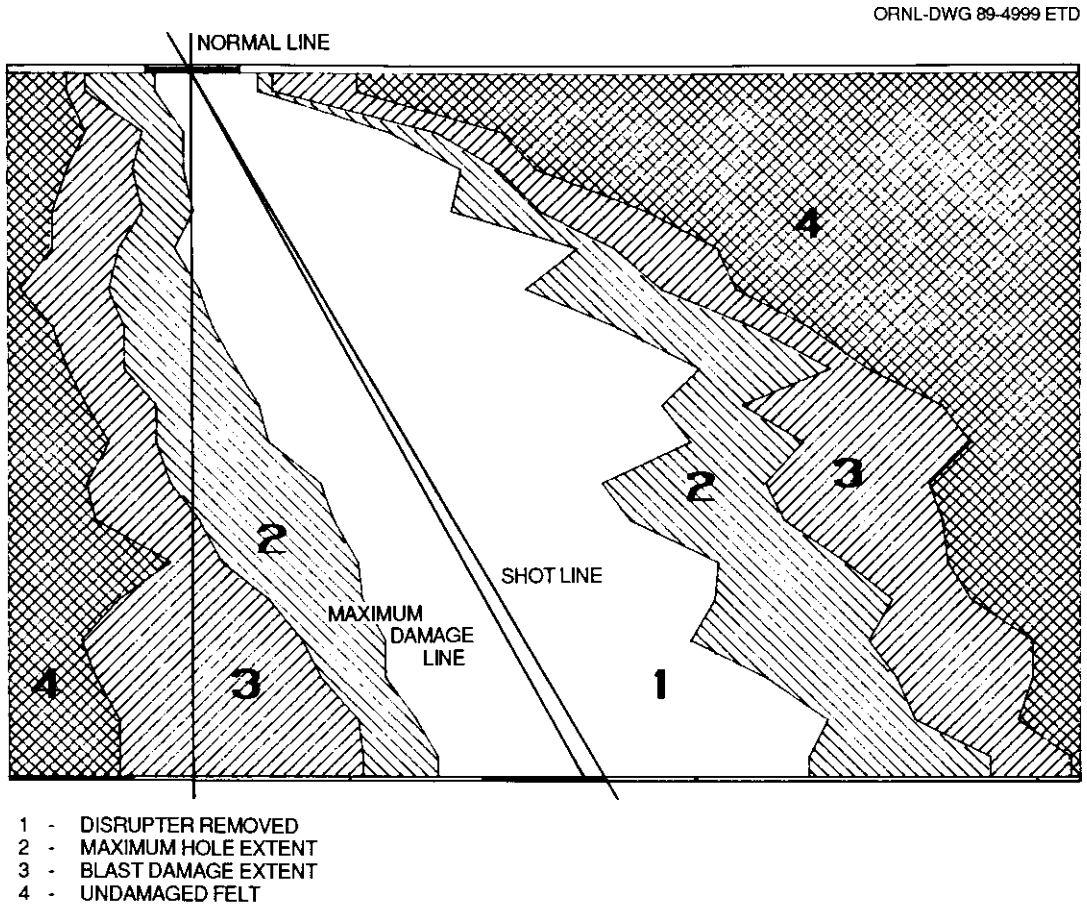


Figure 10. Disrupter blast damage profile for shot 62

penetration damage along the shot line. The line of maximum damage lies between the two damage areas, where the effects have overlapped. For shield 62 (60° incident angle), examination of the damage profile shows only a very slight spall effect, with almost all the damage occurring due to projectile penetration. The line of maximum damage is very close to the continuation of the line of flight. The flash x-ray data for these two tests show the debris clouds while traveling through the disrupter layers, and the phenomena discussed can be seen as it is developing. Figure 11, for shot 61 at 13.1 $\mu$sec, very clearly shows two lobes of damage, one from spall and one from projectile penetration. The direct penetration of the projectile during test 62 can be seen in

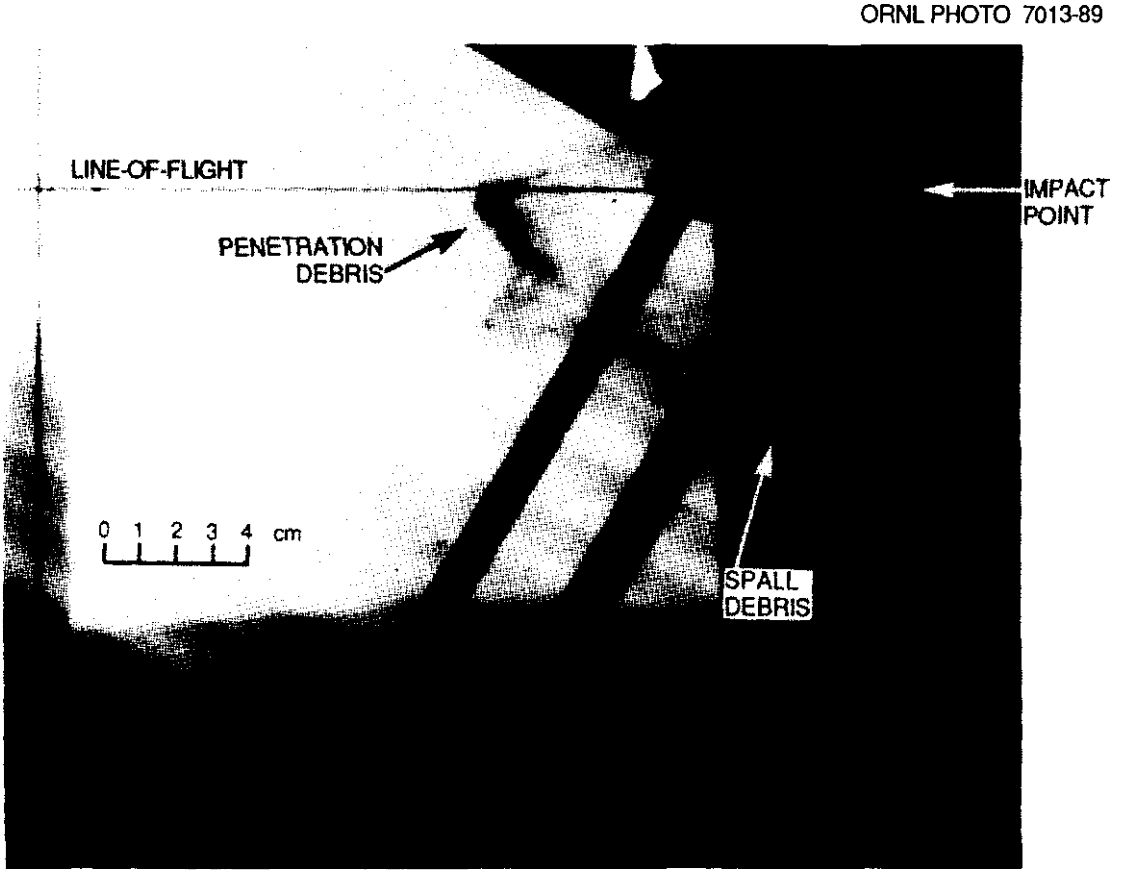


Figure 11. Flash x-ray data for shot 61 at 13.1 μsec

the flash x-ray data, taken at 35.5 μsec, and shown in Figure 12. The deviation of the line of maximum damage from the projectile line of flight appears to increase as the angle of incidence increases, and damage shifts from penetration to spall. This effect is shown in Figure 13, which includes data from shots 61 and 62, another ORNL study (Thomas, 1988) and the Schonberg et al. (1988) study.

Strain gage data at different locations on the back plates was used to compare the relative velocities of the debris clouds. The debris that impacted first on the shield 61 back plate was located almost directly behind the point of impact, indicating that it was part of the spall debris. First impact on the back shield during shot 62 was almost on the line of direct penetration,

ORNL PHOTO 7014-89

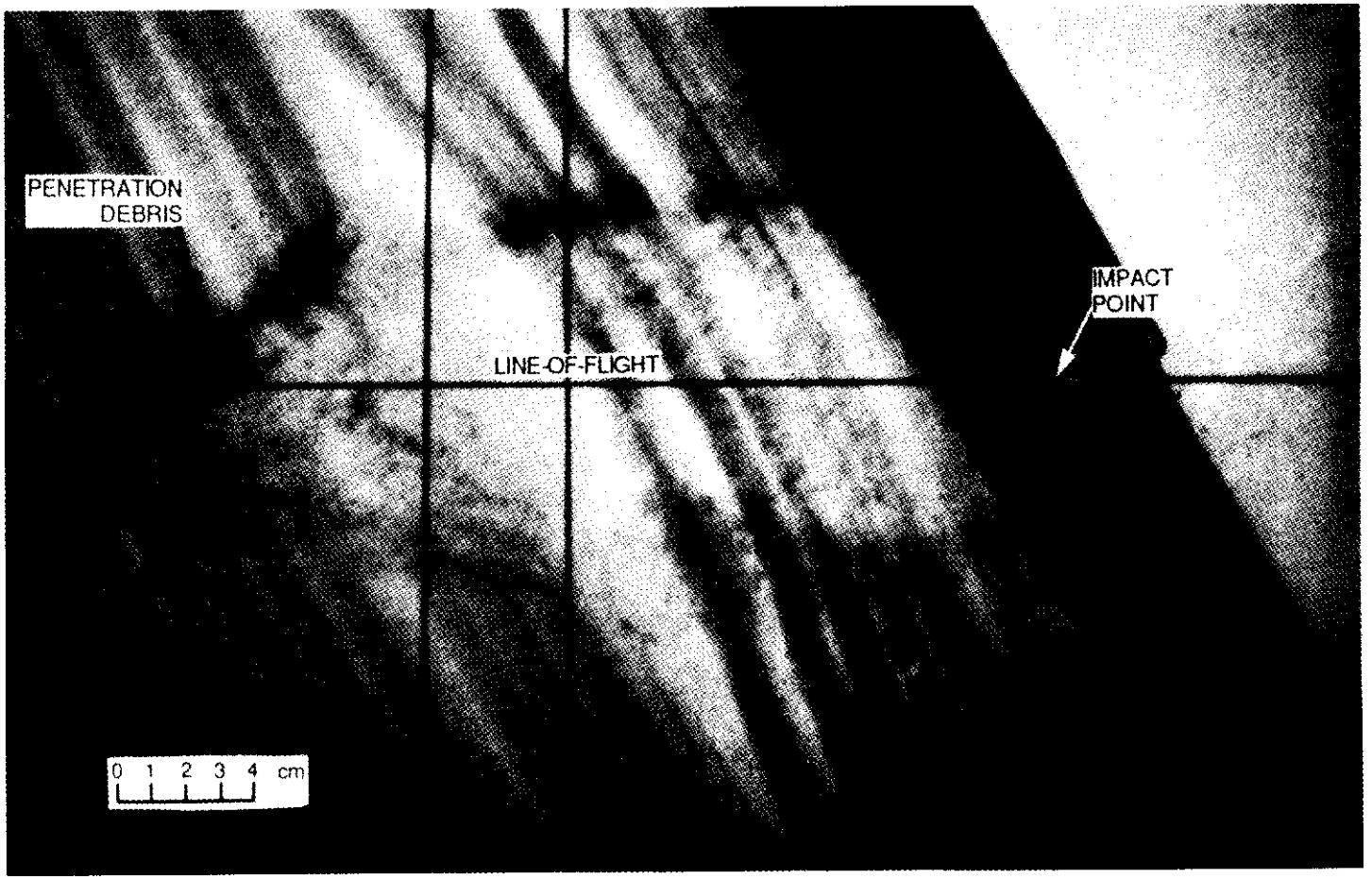


Figure 12. Flash x-ray data for shot 62 at 35.5 $\mu$sec

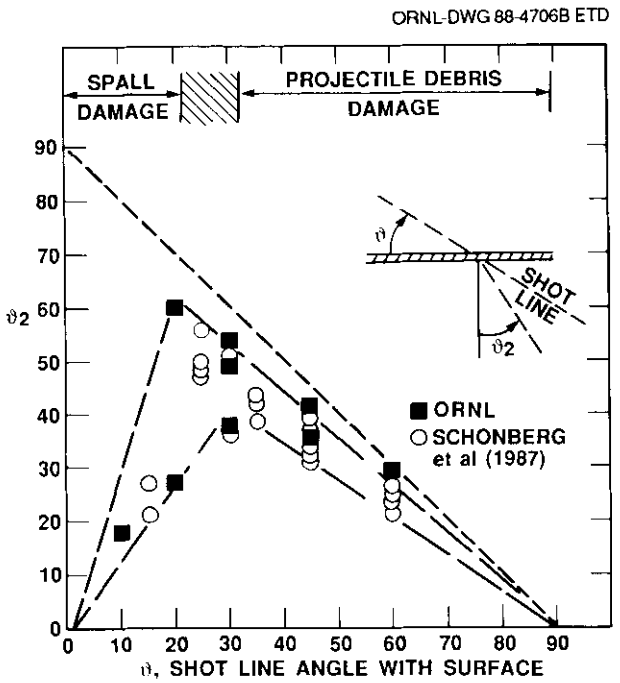


Figure 13. Location of maximum back plate damage versus incidence angle

corresponding with the point of maximum damage to the disrupter and the center of the back plate damage. The first sign of debris impacting the back plate occurred earlier for test 62 than test 61 (see Table 1), but the distance traveled was less in the case of shot 61. This indicates the debris in shot 61 was traveling much slower than the debris in shot 62.

**Table 1. Strain gage data for distance traveled versus time**

| X-RAY DATA | | | | |
|---|---|---|---|---|
| Shot no. | cm (spall) | μsec | cm (projectile) | μsec |
| 61 | 4.3 | 13.1 | 6.5 | 13.1 |
| 62 | 7.6 | 35.5 | 15.9 | 35.5 |
| **BACK PLATE DATA** | | | | |
| Shot no. | cm (spall) | μsec | cm (projectile) | μsec |
| 61 | 15.9 | 46 | 26.5 | 52 |
| 62 | | | 16.3 | 43 |

Back plate damage was widely different for shields 61 and 62. Damage to the back plate of shield 61 was quite minimal, with no overall bulge at all. One small bulge, approximately 1/2 cm in diameter and less than 0.2 cm high, was the only sign of back plate damage. In contrast, the back plate damage for shield 62 was very serious. A general bulge with a 5 1/2 cm by 3 1/2 cm hole having 4 petals resulted from the test. This corresponds to the high level of projectile penetration seen in the x-ray and disrupter layer data. Considering the results for shot 41 with those for shots 61 and 62, back shield survivability can be seen to be a function of the angle of incidence. The same layered shield configuration, tested at different angles, showed widely different results. This is shown in Figure 14, showing the success at 90°, the failure at 60°, and the success at 30°.

A result of the impacts observed during these two oblique impact tests was the presence of a considerable amount of debris generated by the impact which traveled outside the shield. This debris had a definite upstream (greater than ±90° from the projectile line-of-flight) component, as

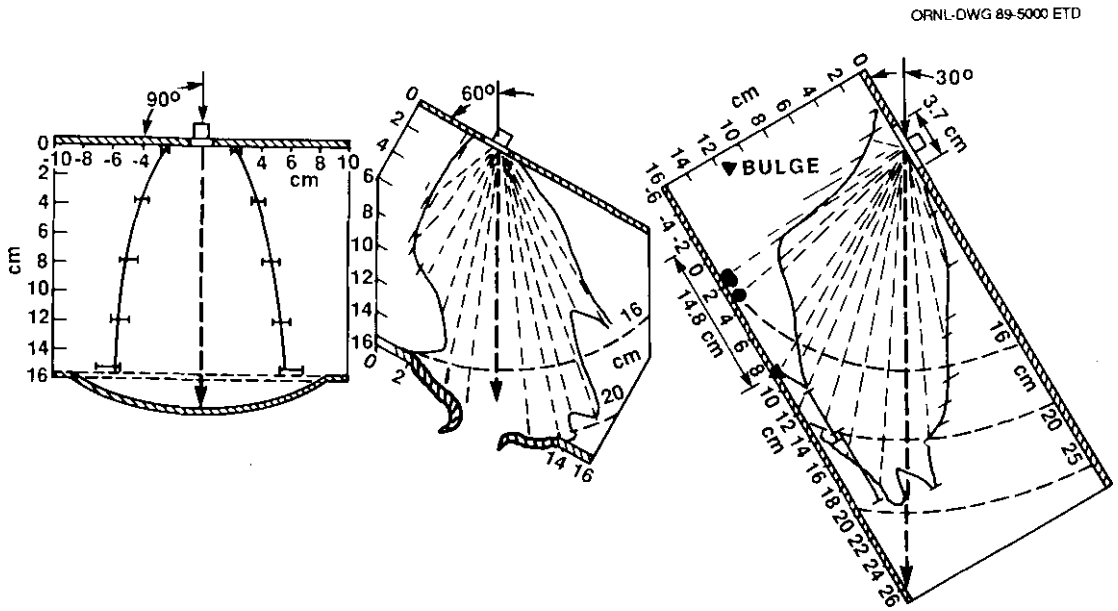


Figure 14. Back shield survivability versus incidence angle

can be seen from the spread of damage on the splash plate, shown in Figure 5. The setup for test 61 did not include a splash plate, so there is insufficient experimental data to fully discuss the generation and spread of the external debris.

## 6. ANALYSIS CONFIGURATIONS AND RESULTS

After the test results showed such a dramatic difference in the results obtained at 30° and 60° incident angles, analyses of the different impact events were performed. The 90° impact case was also modelled as a baseline for comparison. Problem numbers and basic setup information are shown in Table 2. For each case, a cylindrical projectile of the same size and density as the projectile used in testing was modelled. The centerline of the projectile was aligned with the projectile line of flight in each problem to correspond to the assumed "cookie cutter" model.

Very large displacement of localized areas, including penetration, spall, and ejecta, requires that a hydrodynamic computer code or hydrocode be used. The hydrocode makes use of finite difference methods to approximate the solution of the governing partial differential equations. These equations are based on the conservation of mass, momentum, and energy, along with an equation of state and constitutive relationships to properly model the material behavior.

**Table 2. Basic parameters of analysis configurations**

| | | | |
|---|---|---|---|
| Problem No. | 9.01 | 9.616 | 9.612 |
| Incidence angle | 90° | 60° | 30° |
| Corresponding test no. | 41 | 62 | 61 |
| Velocity along flight line, km/s | 7.0 | 7.0 | 6.933 |
| Velocity, in-plane component, km/s | 0 | 3.5 | 6.06 |
| Velocity, normal component, km/s | 7.0 | 6.06 | 3.5 |
| Run time, $\mu$sec | 10.0 | 8.9 | 10.73 |
| Number of cells | 4800 | 76,000 | 152,000 |
| Cell size, cm | 0.075 | 0.10 | 0.05 |

The Eulerian based version of the Hull (Matuska and Osborn, 1987) hydrocode was chosen to model the projectile and front plate impact. The Eulerian version has a framework of cells fixed in space through which material flows. Consequently, very large deformations do not require a remesh or restart as in the Lagrangian or material fixed coordinate systems. The Hull computer code has been widely used in impact studies for a large range of velocities and for a variety of materials. Correlations with experimental data were good for the lexan projectiles first studied in the first phase of this program as reported in the Fast Track Progress Report (ORNL Staff, 1989).

One interesting result obtained from the analytical study was the relative times required for the complete interaction of the projectile with the front plate. Figure 15 shows a series of density plots outlining the development of the hole in the front plate for problem 9.612, the 30° incidence angle case. The hole was still being formed at 4 $\mu$sec after initial contact, and over 10 $\mu$sec were required to obtain the full hole size. The hole development for the 60° case, problem 9.616, is shown in the density plots of Figure 16. Complete hole formation has been obtained by approximately 8 $\mu$sec. In contrast, the front plate hole for the 90° baseline case had become essentially complete before 5 $\mu$sec. (Note: For all color figures, the red/pink areas correspond to high density areas, with shadings down to blue as the low density areas.)

The impact event and resulting projectile penetration/breakup for the baseline 90° case, problem 9.01, are shown in Figure 17. The breakup of the projectile and the condition and spread of the resulting debris cloud for this case are useful for comparison to the results for the oblique impact cases. The debris for the normal impact consists primarily of low density material, with some small separated patches of high density aluminum.

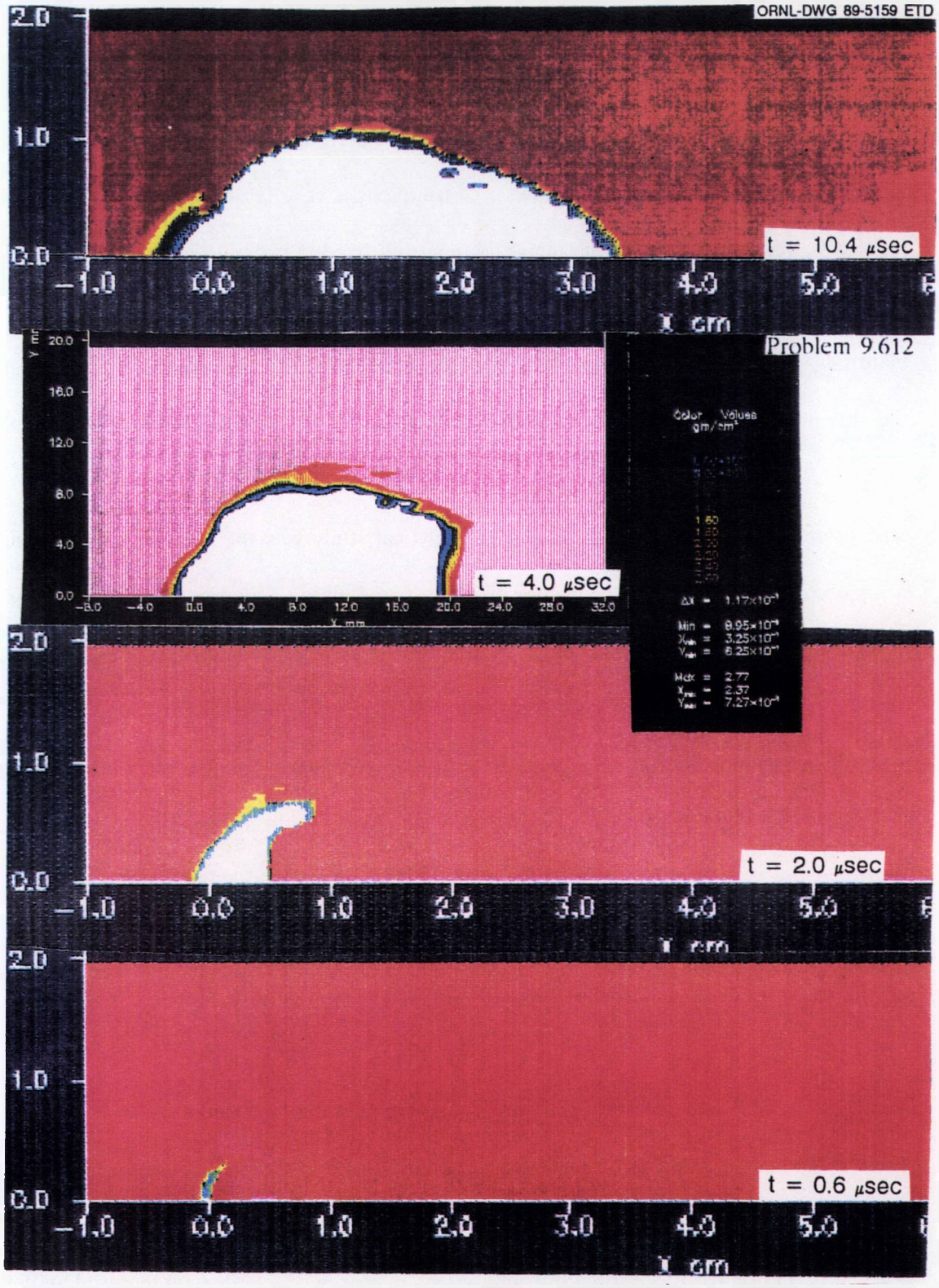


Figure 15. Front plate damage development for a 30° incidence angle

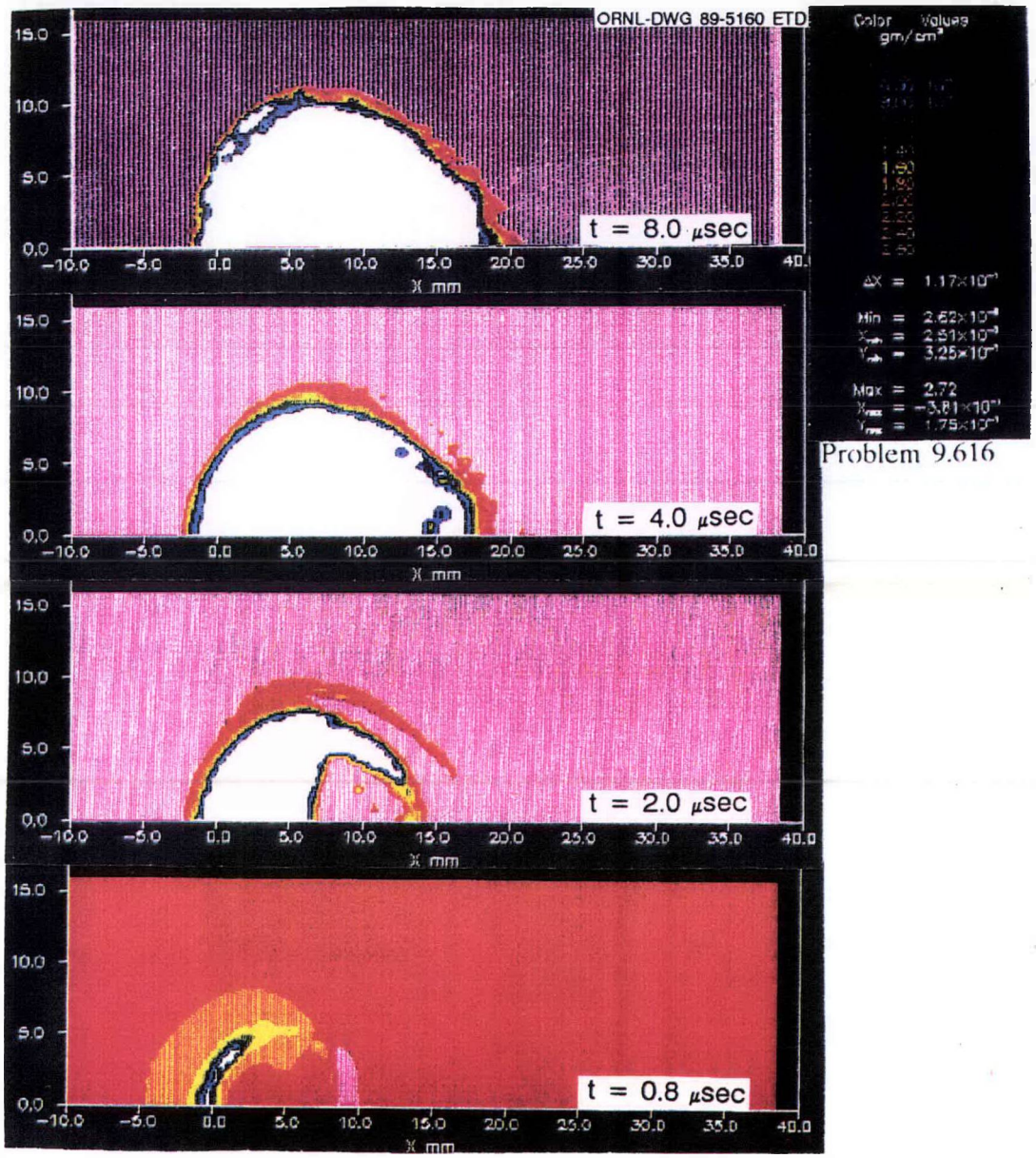


Figure 16. Front plate damage development for a 60° incidence angle

This page was intentionally left blank

DO NOT MICROFILM
THIS PAGE

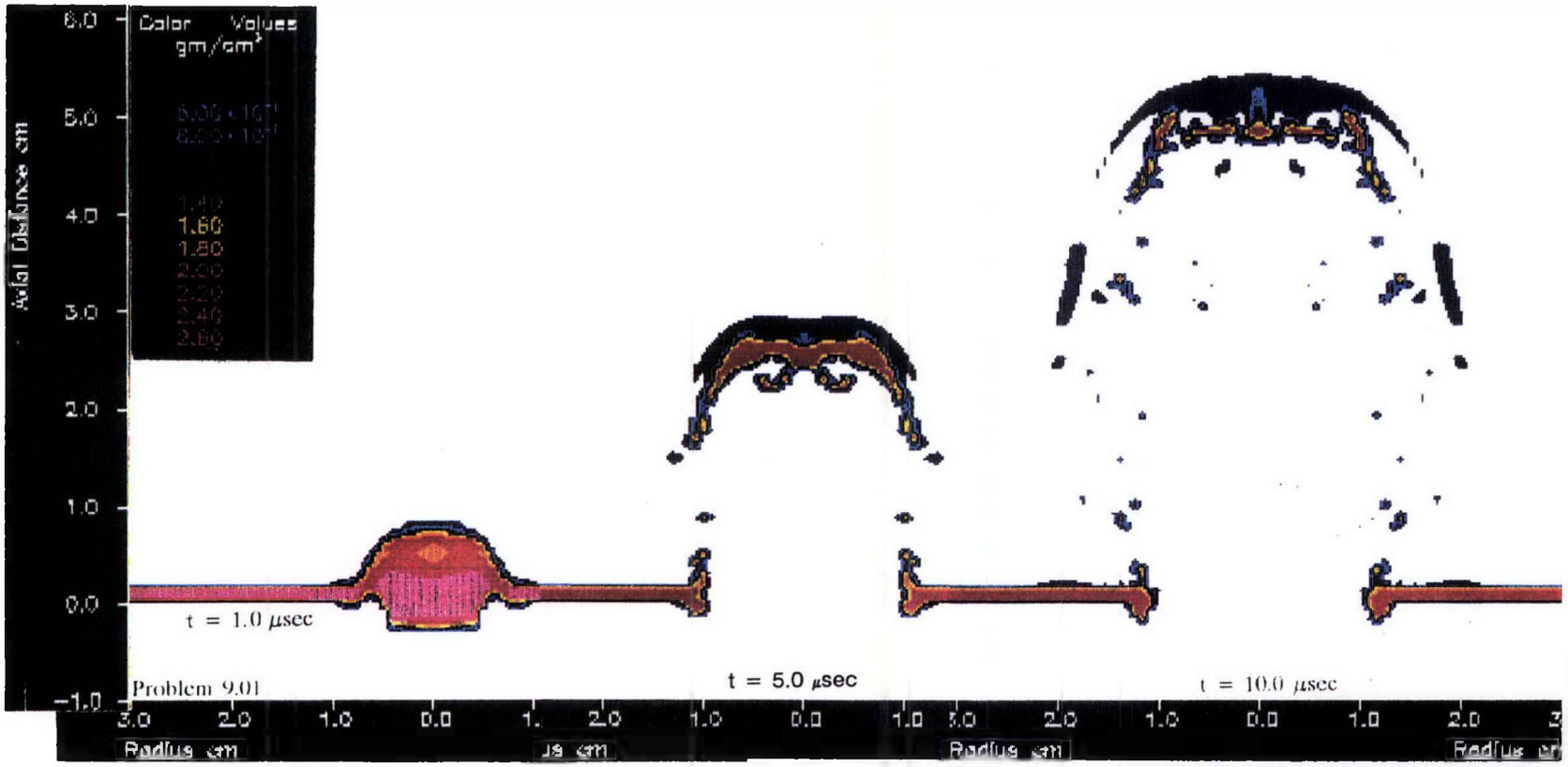


Figure 17. Normal impact debris cloud development

A comparable series of density plots from problem 9.612 (the 30° case) is shown in Figure 18. In comparison with the orthogonal impact event, the debris is generally less broken up. A thicker cap of material is left after penetration, with several small separate high density areas. A significant part of the debris inside the shield appears to be due to spall from the front shield, while the main part of the debris is continuing generally along the shot line. Also, a considerable amount of material is visible outside the shield as ejecta.

Figure 19 is a similar series of density plots for problem 9.616, the 60° incidence angle case. Using the normal impact as a comparison, the debris is again less broken up, with a thick cap containing high density patches of material remaining. However, this result is more pronounced for the 60° case, as a comparison of the debris clouds of Figures 18 and 19 reveals. The amount of high density material left after the 60° impact is much greater, and it is less spread out. Also, due to the angle of direction toward the back plate, the debris for the 60° case has much less distance to travel through and be slowed by the disrupter, increasing the probability for damage to the back plate. The debris for the 60° case, referring again to Figure 19, shows much less spall debris than that of the 30° case.

Further insight into the damage potential of the debris clouds from the different impact cases can be obtained by examination of the velocity vectors for each case. The velocity vectors for problem 9.612 (30°case) at 10 $\mu$sec after impact are shown in Figure 20, both with and without a density plot superimposed. The portion of the debris due to spall and thus moving directly toward the back plate has been drastically reduced in velocity. The debris cloud overall is shown as still somewhat spreading. In contrast, the same type results for problem 9.616 (60° case), given in Figure 21, show that the main section of high density debris is not expanding, but rather is

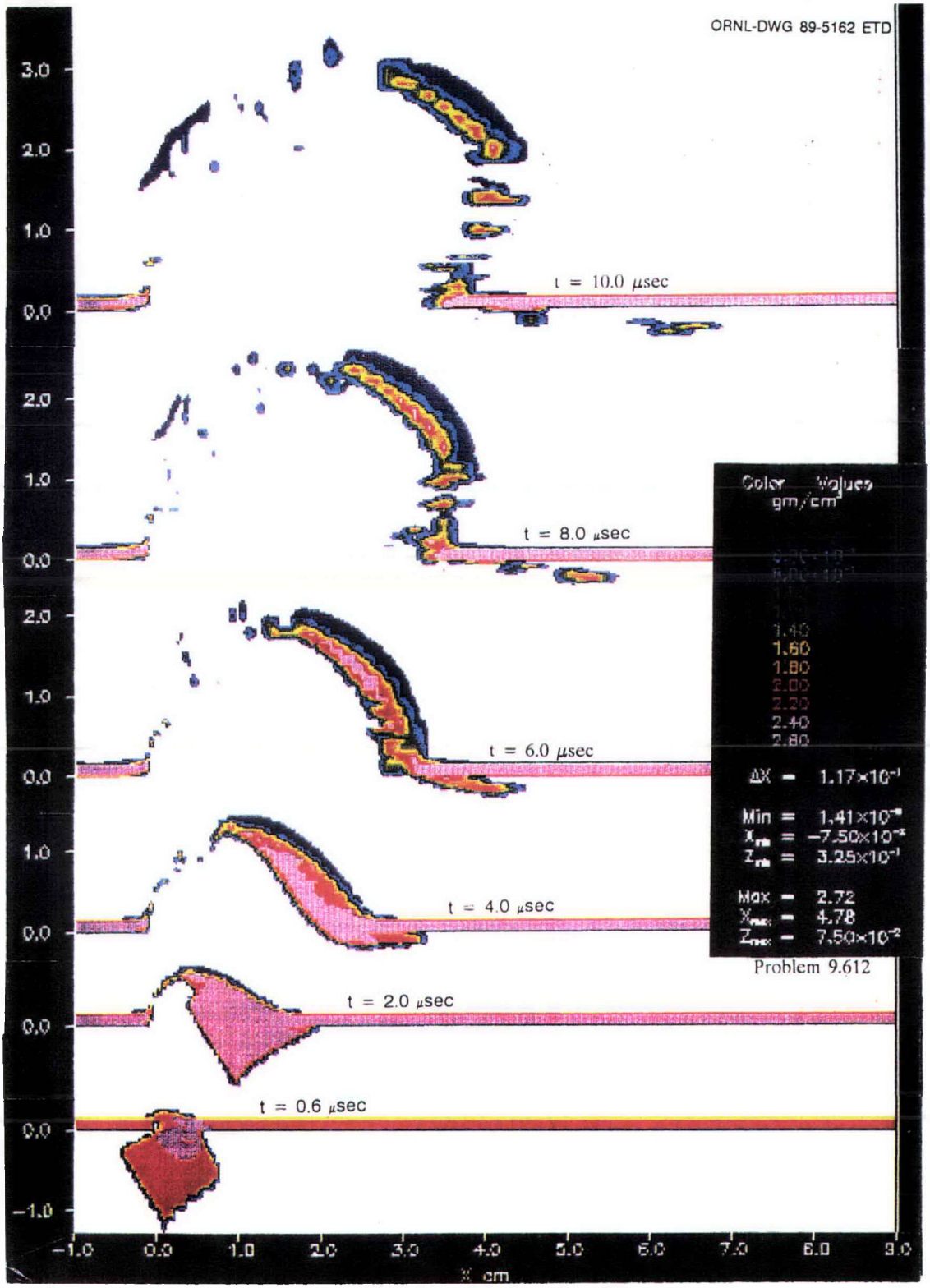


Figure 18. Debris cloud development after a 30° impact

This page was intentionally left blank

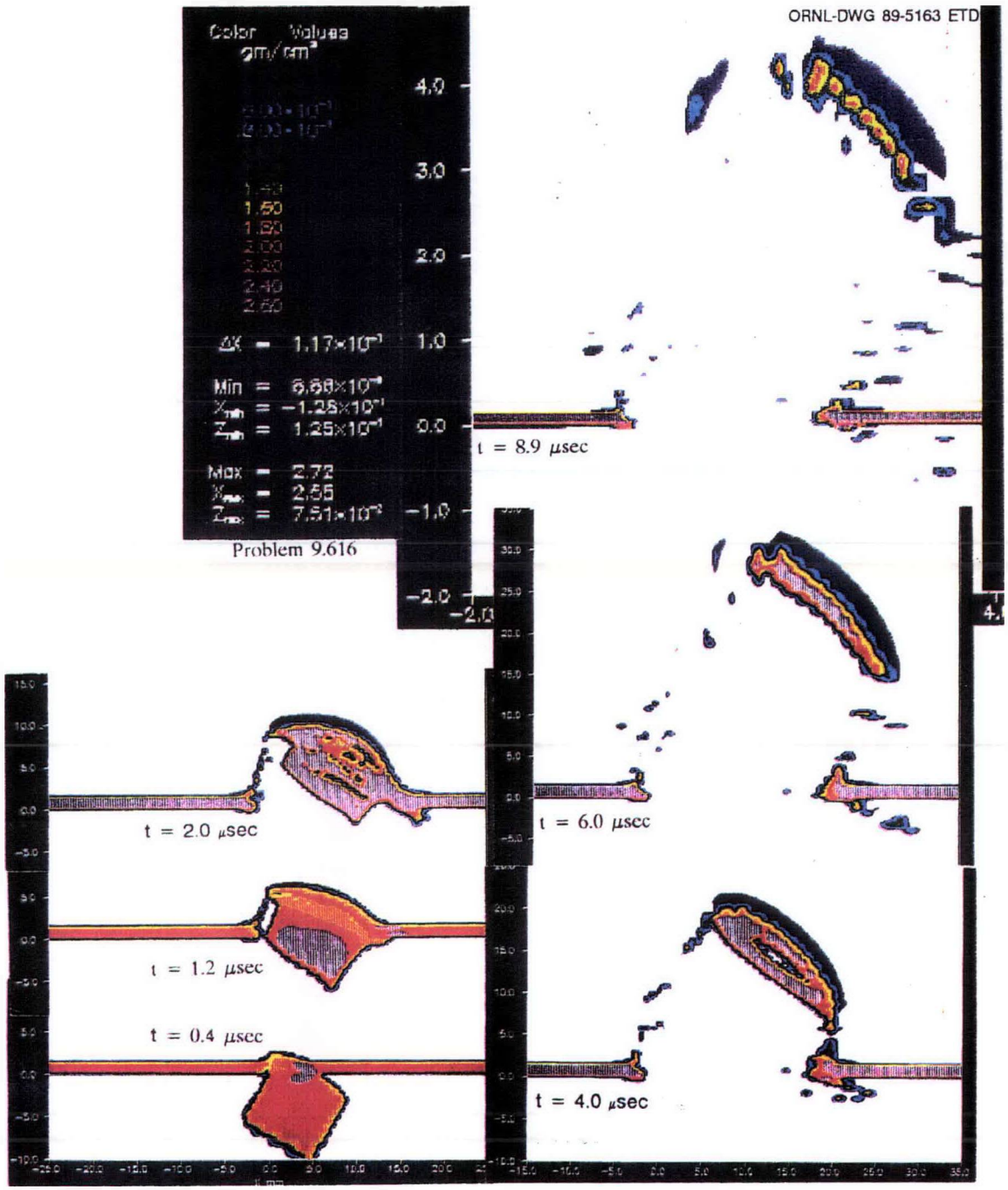


Figure 19. Debris cloud development after a 60° impact

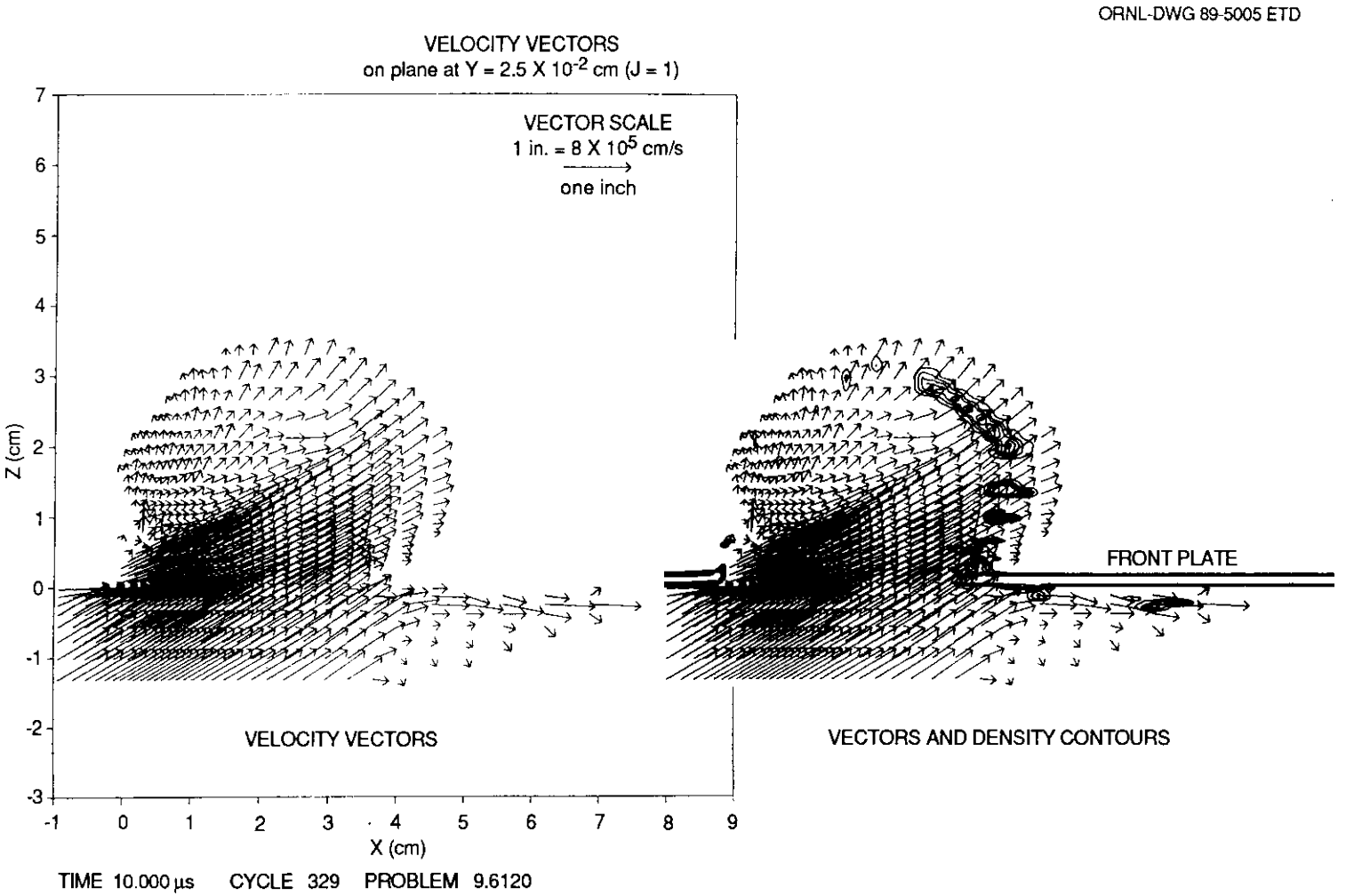


Figure 20. Velocity vectors and debris cloud at 10 $\mu$sec after a 30° impact

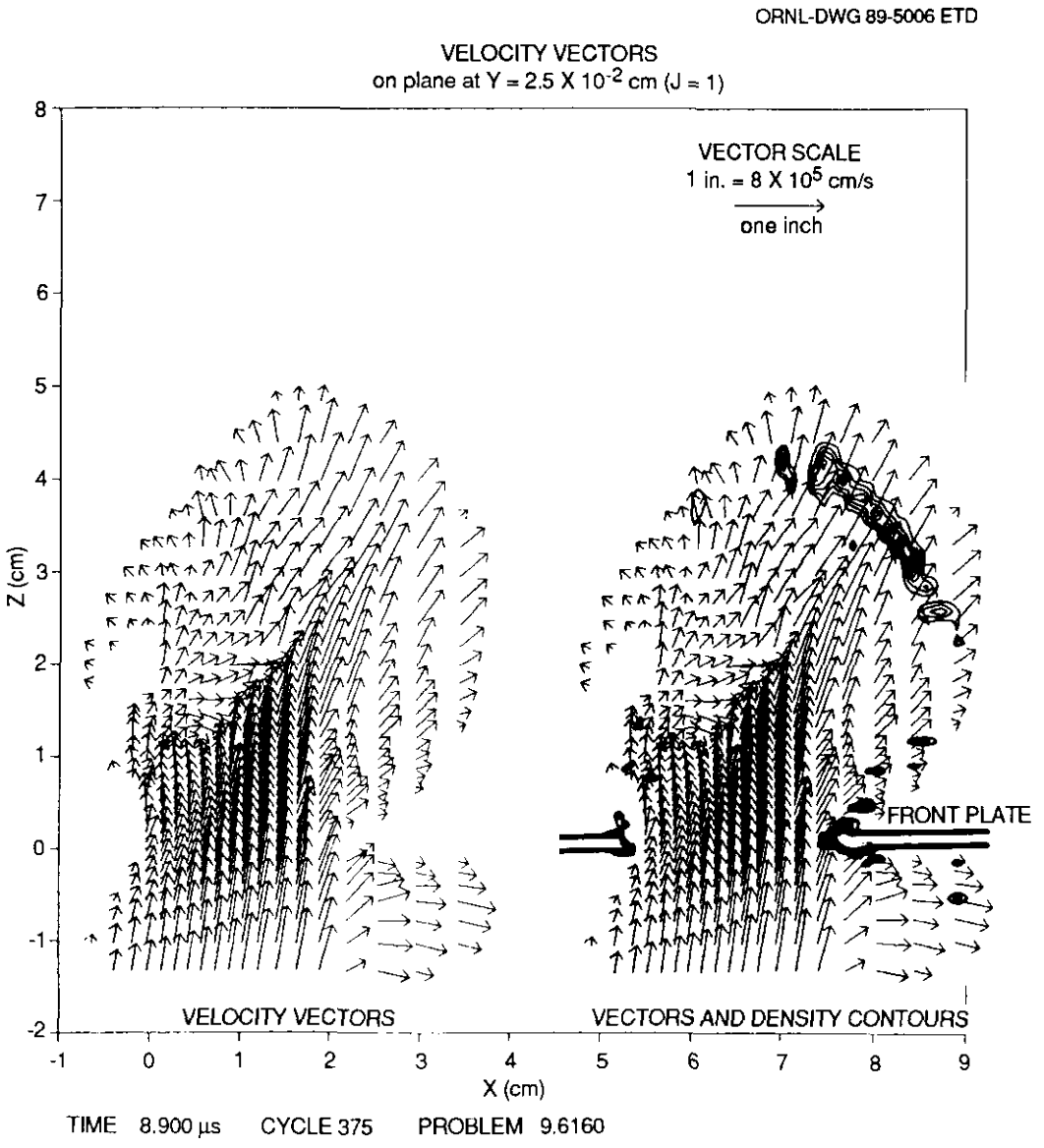


Figure 21. Velocity vectors and debris cloud at 8.9 $\mu$sec after a 60° impact

continuing along the penetration line toward the back plate. Also, the velocity in this 60° case has not been slowed as much as for the 30° case. A very small amount of spall is visible, again moving slowly.

Overall, the analysis results clearly show a much higher damage potential in the debris cloud after the 60° impact than the 30° impact. The debris is of higher density, less dispersed, its velocity is

higher, and the distance to the back plate is less. For both oblique impacts, the projectile is less broken up than in the normal impact case. However, the debris for the 30° case is more dispersed, having a more significant spall component than the 60° case. The amount of debris outside the shield is greater and contains more dense material in the 30° case, showing a higher damage potential outside the shield.

## 7. COMPARISON OF ANALYSIS AND TEST RESULTS

Direct comparison of the analytical and experimental results can be made in three major areas:

1. The experimental results for front plate damage, previously shown in Figure 6, correspond well with the analytical results obtained. Table 3 shows the comparison of the two in terms of major and minor axis measurements, with the normal case diameter included also. In Figures 22 and 23, the analytical results for the 30° and 60° degree incidence angles are shown with the experimental results superimposed.
2. Analytically obtained density plots of the debris clouds show a much more pronounced spall damage area for the 30° case than for the 60° case, referring to Figures 18 and 19. This corresponds very well with the damage profiles seen in the disrupter, both during the test in the flash x-ray data (Figures 11 and 12) and afterwards in the remaining damage profiles (Figures 9 and 10).
3. The high potential for damage seen as an overall result of the analysis of the 60° case matches well with the back plate failure that resulted from shot 62. The lower damage potentials of

**Table 3. Comparison of analytical and experimental front plate damage**

| Test no. | | 41 | 61 | 62 |
|---|---|---|---|---|
| Problem no. | | 9.01 | 9.612 | 9.616 |
| Incidence angle | | 90° | 30° | 60° |
| **HOLE DIAMETER** | | | | |
| Maximum, cm | analytical | 2.4 | 3.5 | 2.0 |
| | experimental | 1.9 | 3.6 | 2.25 |
| **HOLE DIAMETER** | | | | |
| Minimum, cm | analytical | 2.4 | 2.2 | 1.93 |
| | experimental | 1.75 | 2.2 | 1.90 |

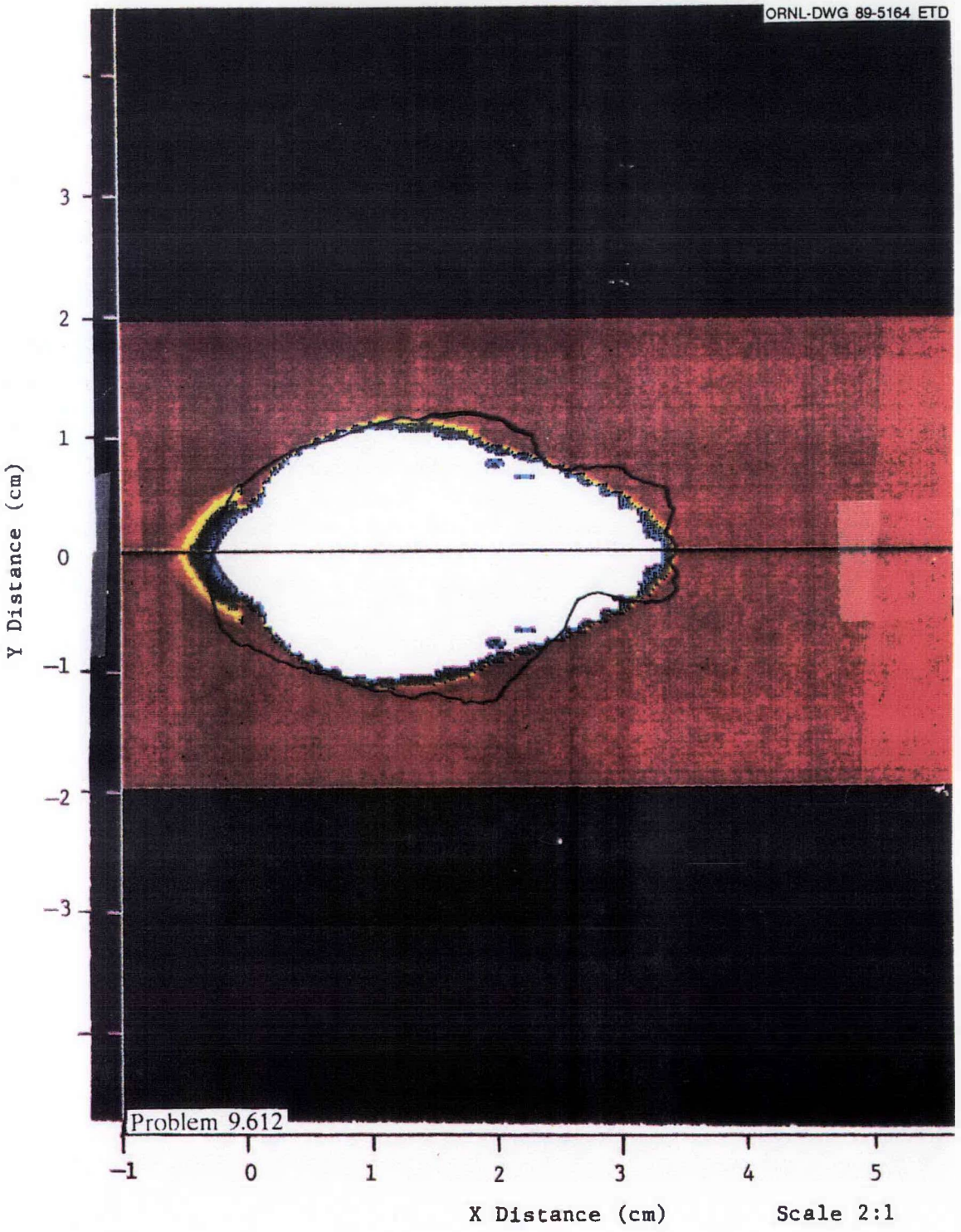


Figure 22. Analytical and experimental front plate damage from a 30° impact

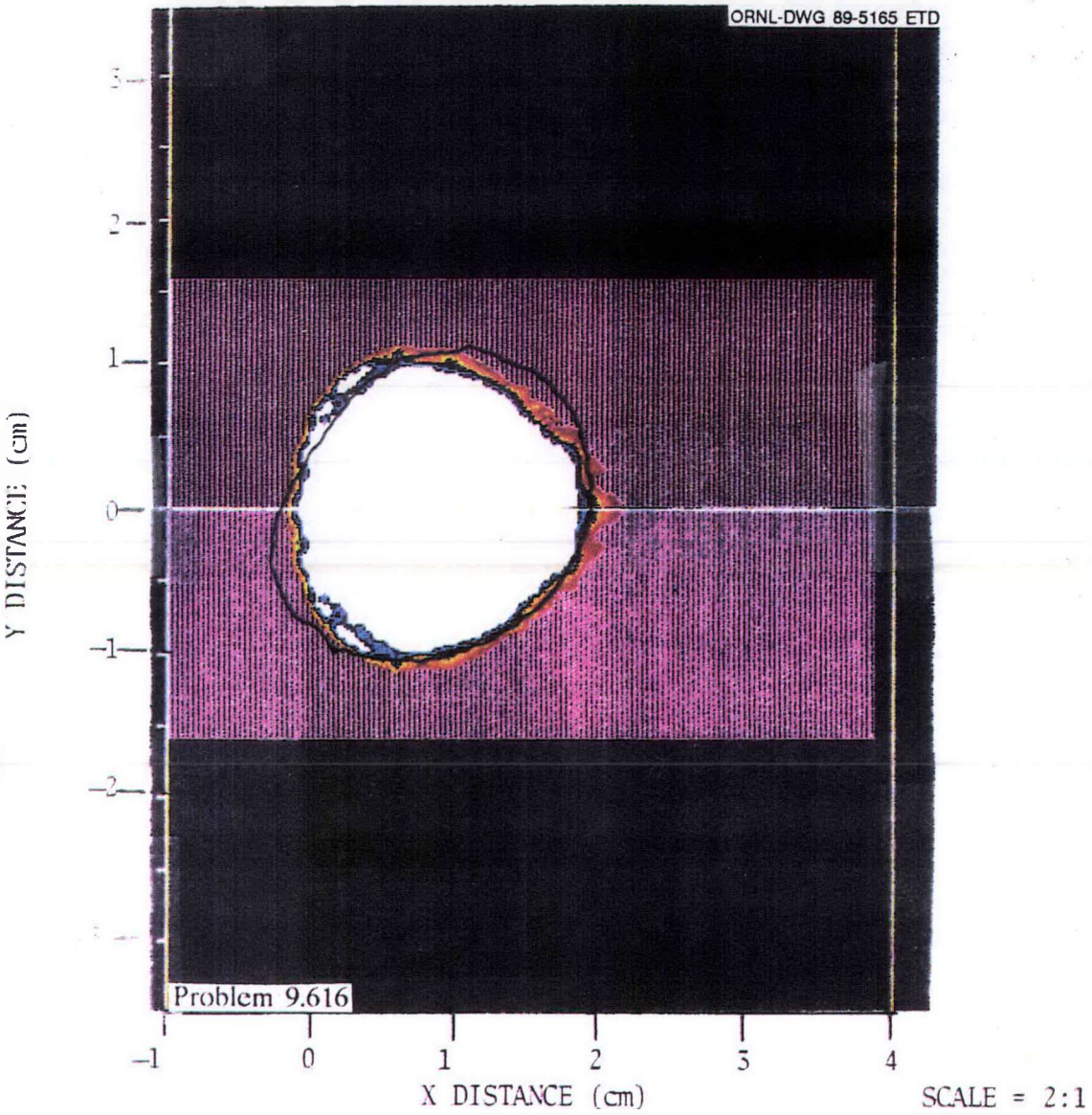


Figure 23. Analytical and experimental front plate damage from a 60° impact

the normal case and the 30° case are in agreement with the low levels of back plate damage seen in tests 41 and 61, in which the back plates did not fail.

Preliminary comments only can be made with regard to the external debris generated. The analysis showed debris outside the shield, referring to problem 9.616 as shown in Figure 19, and this is in general agreement with the results seen on the splash plate for the 60° test. However, analytical results indicate a greater amount of splash for a 30° incidence angle impact, especially in the downstream (within ±90° of the projectile line-of-flight) direction. This is indicative of a higher damage potential outside the shield and possibly also indicative of incipient ricochet if the incidence angle is further reduced. No experimental results for the external damage due to the 30° impact were obtained in this study. These analytical results do correspond with those seen in the studies by Schonberg et al. (1988) and Thomas (1988) in which the external damage did increase as the incidence angle decreased.

# 8. CONCLUSIONS AND RECOMMENDATIONS

There are four significant conclusions that result from this study:

1. Front plate damage from hypervelocity impact varies significantly with the incidence angle. Damage to the front plate was much greater at a 30° incidence angle than at a 60° incidence angle, and the minimum front plate damage occurred for the 90° impact case.
2. Damage internal to the shield results from two phenomena, the occurrence of spall debris from the back of the front shield directly behind the impact and the penetration and breakup of the projectile along the original line of flight. At the time of initial impact, a normal compressive wave is sent through the front shield with a velocity characteristic of the normal velocity. When this wave is reflected as a tension wave from the back surface of the front shield, spall may or may not occur. If spall is created, its path will be generally perpendicular to the front shield and thus differ from the debris created by penetration of the projectile. The relative amounts, velocities, and spread of the debris from these two phenomena are also a function of incidence angle.
3. Back plate damage varies significantly with incidence angle. A much greater amount of back plate damage occurred for a 60° incidence angle than for either a 30° or a normal impact. The back plate failed, having a large petalled hole at 60°, while damage for the 30° incidence angle test was negligible. A definite overall bulge but no spall or penetration occurred for the shield tested against the 90° incidence projectile. A layered composite shield which survives a normal impact thus may fail against the same projectile at a different incidence angle.
4. Debris generated external to the shield is also dependent on the incidence angle. Preliminary indications are that the damage potential of this type of debris increases as the projectile angle of incidence decreases.

Several recommendations for further study, both analytical and experimental, are listed below:

1. The dependence of the five types of damage discussed above (front plate, internal damage as spall, internal damage as projectile penetration, back plate damage, and external debris generation) on the incidence angle of the projectile needs to be more clearly defined. The interrelation of these effects is also of interest. Further testing and analyses similar to the preliminary results described here would help provide this information.
2. Another area of interest is the relationship between the damage produced and the yaw angle of the incoming projectile. (Yaw angle is the angle between the axis of the cylindrical projectile and the line-of-flight of the projectile.) The combination of incidence angle dependence and yaw angle effects should be studied further, again with more testing and analyses.
3. The shield configurations tested in this study were all identical. There are many questions left concerning the relationship between the different shield components and their response to different incidence angles; e.g., the spacing between the front and back shields necessary for a successful shield may also be a function of incidence angle. Ricochet may occur at different incidence angles for different combinations of projectile and front plate materials. Front plate thickness is known to be a very important parameter in hypervelocity shield performance. The relationship between front plate thickness and projectile breakup as a function of different incidence angles should be studied further, again for different combinations of projectile and front plate materials. Further testing and analyses are recommended again.
4. The effects of oblique impact on momentum multiplication (relationship between size and velocity of the debris created) are not known. This area needs study.

## 9. REFERENCES

Cable, A. J., "Experimental Studies of Hypervelocity Impact with the R.A.R.D.E. 1/4 IACH Calibre Launches," *Fluid Dynamics Aspects of Space Flight*, Vol.1, Gordon and Breach Science Publishers, pp. 331-334, 1965.

Gehring, J. W., in *High Velocity Impact Phenomena*, pp. 463-514, Ed. by Ray Kinston, Academic Press, 1970.

Matuska, D. A. and Osborn, J. I., *Hull Hydrocode Documentation, User's Manual*, published 1983, revised October 1987 by Orlando Technology Inc., Shaliman, Florida.

Merzhievskii, L. A. and Urushkin, V. P., "Oblique Collision of a High Speed Particle with a Shield," *Combustion, Explosion and Shock Waves*, Vol. 16, pp. 551-555, 1980.

ORNL Staff, "Technical Progress on the ORNL Fast Track Defensive Shield Demonstration Program for the Period April 1986 - September 1987 (U)," ORNL TM-10630, 1989.

Orphal, D. L., Wagner, H. M., and Vivian, C. E., "Low Angle Impact and Penetration of Thin-Laminated Targets by Spheres," Proceedings of 1982 Symposium on Ballistics, ADPA, November 1982.

Schonberg, W. P., Taylor, R. A., and Horn, J. R., "An Analysis of Penetration and Ricochet Phenomena in Oblique Hypervelocity Impact," NASA TM-100319, Marshall Space Flight Center, February 1988.

Smith, J. E., "Experimental Methods," ORNL TM -----, in press.

Summers, J. L., "Evaluation of the Impact Performance of Realistic Space Structures," *Fluid Dynamics Aspects of Space Flight*, Vol.1, Gordon and Breach Science Publishers, pp. 299-314, 1965.

Thomas, D. G., Brewer, E. D., Hendrich, W. R., and Smith, J. E., "Front Plate and Projectile Variance Effects," ORNL TM -----, in press.

## INTERNAL DISTRIBUTION

1. D. E. Bartine
2. E. D. Brewer
3. D. W. Burton
4. J. M. Corum
5. E. B. Harris
6. W. R. Hendrich
7. R. L. Huddleston
8. D. T. Ingersoll
9. J. E. Jones Jr.
10. F. C. Maienschein
11. R. T. Santoro
12. J. E. Smith
13. D. G. Thomas
14. ORNL Patent Office
15. Central Research Library
16. Document Reference Section
17. Laboratory Records
18. Laboratory Records (RC)

## EXTERNAL DISTRIBUTION

19. Dr. Charles Aeby, AFWL/NTC, Air Force Weapons Laboratory, Kirtland Air Force Base, New Mexico 87117-6008

20. Dr. M. Alme, Computer Sciences Corporation, 2100 Air Park Road SE, Albuquerque, New Mexico 87106

21. Lt. Dale Atkinson, AFWL/NTCA, Air Force Weapons Laboratory, Kirtland Air Force Base, New Mexico 87117-6008

22. Mr. L. Bariess, Martin Marietta Denver Aerospace, P.O. Box 179, Denver, Colorado 80201

23. Bob Becker, U.S. Army Strategic Defense Command, 106 Wynn Drive, SLKT, Huntsville, Alabama 35805

24. Mr. B. Belason, AVCO Specialty Materials, 2 Industrial Way, Lowell, Massachusetts 01851

25. Dr. C. Bersch, Institute for Defense Analysis, 1801 N. Beauregard Street, Alexandria, Virginia 22311

26. R. L. Bjork, PACTECH, P.O. Box 148, Del Mar, California 92014

27. Stan Brockway, Kaman Sciences Corporation, 600 Boulevard South, Huntsville, Alabama 35805

28. Carl Chambers, CSSD-H-LL, U.S. Army Strategic Defense Command, 106 Wynn Drive, Huntsville, Alabama 35805

29. CMDR J. C. Connell, Defense Nuclear Agency, 6801 Telegraph Road, Alexandria, Virginia 22310

30. W. E. Cooper, IN-I, U.S. Army Strategic Defense Command, 106 Wynn Drive, Huntsville, Alabama 35805

31. Dr. B. Cour-Palais, NASA Johnson Space Center, Houston, Texas 77058

32. Jeanne Crews, NASA Johnson Space Center, SN-31, Houston, Texas 77058

33. DETIR, Kaman Sciences Corporation - TEMPO Division, 2560 Huntington Avenue, Suite 500, Alexandria, Virginia 22303-1490

34. DETIR, Kaman Sciences Corporation - TEMPO Division, 816 State Street, P.O. Drawer QQ, Santa Barbara, California 93102-1479

35. James Eamon, Kaman Sciences Corporation, 1500 Garden of the Gods Road, Colorado Springs, Colorado 80933

36. Tosh Fujita, Jet Propulsion Laboratory, 4800 Oak Grove Drive, Pasadena, California 91109

37. Dr. W. Isbell, General Research Corporation, P.O. Box 30400, Santa Barbara, California 93105

38. Richard Jackson, Kaman Sciences Corporation, 600 Boulevard South, Huntsville, Alabama 35805

39. Dick Keefee, Kaman Sciences Corporation, 1500 Garden of the Gods Road, Colorado Springs, Colorado 80933

40. George Landwehr, Teledyne Brown Engineering, 300 Sparkman Drive, Huntsville, Alabama 35807

41. John La Ulibarri, Sandia National Laboratory, 1515 Eubank Boulevard SE, P.O. Box 5800, Albuquerque, New Mexico 87185

42. R. J. Lawrence, Div. 9014, Sandia National Laboratory, 1515 Eubank Boulevard SE, P.O. Box 5800, Albuquerque, New Mexico 87185

43. Lt. Col. C. Lee, SD/CNIV, P.O. Box 92960, Los Angeles Air Force Base, Los Angeles, California 90009-2960

44. Dr. Julius Lilly, U. S. Army Strategic Defense Command, 106 Wynn Drive, CSSD-H-LL, Huntsville, Alabama 35805

45. Dr. J. E. Lowder, SPARTA, Inc., 21 Worthen Road, Lexington, Massachusetts 02173

46. Maj. Thomas McDowell, SDIO/T/SL, Pentagon, Washington, D.C. 20301-7100

47. Dr. W. G. Nichols, Computer Sciences Corporation, 2100 Air Park Road SE, Albuquerque, New Mexico 87106

48. Dr. J. J. O'Sullivan, ANSER Corporation, 1215 Jefferson Davis Hwy., Suite 800, Arlington, Virginia 22202

49. Glenn Ormbrek, AFWAL/MLLN, Wright Research and Development Center, Wright-Patterson Air Force Base, Ohio 45433-6533

50. Glenn Pomykall, Lawrence Livermore National Laboratory, P.O. Box 808, Livermore, California 94550

51. George Schmidt, AFWAL/MLPJ, Wright Research and Development Center, Wright-Patterson Air Force Base, Ohio 45433-6533

52. Dr. William P. Schonberg, Mechanical Engineering Department, University of Alabama at Huntsville, Huntsville, Alabama 35899

53. Dr. P. Seckler, SD/CNWK, P.O. Box 92960, Los Angeles Air Force Base, Los Angeles, California 90009-2960

54. William Tedeschi, Sandia National Laboratory, 1515 Eubank Boulevard SE, P.O. Box 5800, Albuquerque, New Mexico 87185

55. John Tipton, HNDED-SY, U.S. Army Engineering Division, P.O. Box 1600, Huntsville, Alabama, 35807-4301

56. Dr. R. Washburn, SPARTA, Inc., 21 Worthen Road, Lexington, Massachusetts 02173

57. A. E. Williams, Naval Research Laboratory, Washington, D.C. 20375

58. Office of Asst. Manager for Energy Research and Development, DOE-ORO, Oak Ridge, TN 37831

59-60. Office of Scientific and Technical Information, P.O. Box 62, Oak Ridge, Tennessee 37830